Distinct effects of Fine and Coarse Aerosols on Microphysical Processes of Shallow Precipitation Systems in Summer over Southern China

Fengjiao Chen [1,2], YuanjianYang[3*], Lu Yu[1], Yang Li[1], Weiguang Liu [1], Yan Liu [1,4], Simone Lolli[5]

[1] *Key Laboratory of Transportation Meteorology of China Meteorological Administration, Nanjing Joint Institute for Atmospheric Sciences, Nanjing, China*

[2] *China Meteorological Administration Radar Meteorology Key Laboratory, Beijing, China*

[3] *School of Atmospheric Physics, Nanjing University of Information Science and Technology, Nanjing, Jiangsu, China*

[4] *State Key Laboratory of Severe Weather, Chinese Academy of Meteorological Sciences, Beijing, China.*

[5] *CNR-IMAA, Contrada S. Loja, 85050 Tito Scalo (PZ), Italy*

**Corresponding author: Prof. Yuanjian Yang (yyj1985@nuist.edu.cn)*

Abstract: The densely populated South China, adjacent to the South China Sea, which is associated with shallow precipitation during summer, is an open-air natural laboratory for studying the impact of aerosol particles on shallow precipitation events. Using eight years of data from dual-frequency precipitation radar measurements, aerosol reanalysis, and atmospheric reanalysis, this study investigates the potential influence of coarse and fine aerosol particles on the structure of the precipitation and the microphysical processes of shallow precipitation in South China. Statistical results indicate that during coarse aerosol-polluted conditions, shallow precipitation clouds have a lower mean height of the storm top (STH, ~3.2 km), but a higher mean near-surface rainfall (RR, ~1.78 mm h^{-1}), characterized by high concentrations of large raindrops, driven mainly by significant collision-coalescence processes (accounting for 74.1%). In contrast, during fine aerosol-polluted conditions, shallow precipitation clouds develop a deeper median STH ~3.7 km with lower surface RR characterized by a low concentration of small raindrops, resulting from increased breakup processes (33.1%) and reduced collision-coalescence processes (69.6%). The coarse (fine) aerosol particles act as promoters (inhibitors) of radar reflectivity in the profile of shallow precipitation, regardless of dynamic and humid conditions. The effect of coarse aerosol particles in promoting precipitation and the inhibiting effect of fine aerosol particles are the most significant under low humidity conditions, mainly attributed to significantly enhanced collision-coalescence processes, exceeding 22.2%. Furthermore, the increase in RR above 3 km during coarse aerosol-polluted environments is mainly driven by the high concentration of hydrometeors in low instability conditions, whereas by large hydrometeors in high instability environments.

Short Summary: The microphysical mechanisms of precipitation responsible for the varied impacts of aerosol particles on shallow precipitation remain unclear. This study reveals that coarse aerosol particles invigorate shallow rainfall through enhanced coalescence processes, whereas fine aerosol particles suppress shallow rainfall through intensified microphysical breaks. These impacts are independent of thermodynamic environments, but are more significant in low-humidity conditions.

1 Introduction

Shallow precipitation, generally identified by storm height, dominates in marine regions such as the ocean and coastal continent, potentially accounting for 20% of rainfall over tropical oceans and 7.5% over tropical land (Liu and Zipser, 2009; Chen et al., 2016; Short and Nakamura, 2000). This underscores its crucial significance in the regulation of the global water cycle. However, shallow precipitation is a complex phenomenon influenced by various factors such as water vapor, thermodynamic environment, and aerosol particles (Lang et al., 2021; Chen et al., 2024; Smalley and Rapp, 2020). Aerosol particles, as one of these factors, have sparked significant debate due to the intricate nature of aerosol-radiation and aerosol-cloud interactions among various species, resulting in unanswered questions about whether aerosol particles will increase or decrease shallow precipitation (Koren et al., 2014; Fan et al., 2020; Christensen and Stephens, 2012).

The impact of aerosol particles on precipitation has been widely investigated in many previous studies (Sun and Zhao, 2021; Miltenberger et al., 2018; Liu et al., 2022; Fan et al., 2018). Regional differences show that aerosol particles can delay the start time of precipitation by 2 hours in the Pearl River Delta but advance by 3 hours in the North China Plain (Sun and Zhao, 2021). Furthermore, precipitation is suppressed for stratocumulus and small cumulus clouds in highly polluted environments, but enhanced for heavy precipitation events and deep convective clouds (Yuan et al., 2011; Rosenfeld et al., 2008; Xiao et al., 2022; Miltenberger et al., 2018). However, convective rainfall invigoration depends on aerosol concentrations, which turns into suppression at the turning zone of aerosol optical depth in 0.25-0.30 (Guo et al., 2019), potentially linked

to a change from aerosol microphysical effects to aerosol radiative effects (Jiang et al., 2016). Liu et al. (2022) examined various aerosol types and discovered that marine warm clouds experienced a fourfold increase in rainfall flux in the presence of high levels of coarse spray aerosol particles, while there was a reduction by 75% in conditions with high concentrations of fine aerosol particles. Additionally, these contrast effects are independent of meteorological conditions. Another study suggests that the improvement of rainfall in orographic regions with high mineral dust concentrations is more significant in humid environments (Zhang et al., 2020b). Overall, the effects of aerosol particles on precipitation depend on numerous elements such as weather conditions, types of aerosol particles, their concentration, types of clouds, among others, and thus need to be carefully analyzed.

Most of these studies on the interactions between aerosol particles and precipitation have focused on the intensity, frequency of precipitation, and start and peak times of precipitation, but few studies have reported on how aerosol particles impact rainfall through modulating microphysical structures and processes of precipitation. Using three-dimensional observations of precipitation and microphysics from dual frequency precipitation radar (DPR) onboard the Global Precipitation Mission (GPM), recent studies have revealed that aerosol particles mainly reduce mean droplet concentration and increases the effective radius of precipitation in most regions of eastern China (Sun et al., 2022), except Northeast China as Xiao et al. (2022) found that the aerosol invigoration effect on convective rainfall is characterized by higher droplet concentration with smaller size under polluted conditions in Northeast China. However, the impact of different aerosol species on precipitation microphysical structures and microphysical processes (i.e., coalescence efficiency of rain droplets) has been scarcely examined, which is essential for comprehending the full picture of the connections between aerosol particles, precipitation microphysics, and precipitation.

South China (18~29°N, 110~123°E) is a region where shallow precipitation occurs frequently (occurrence frequency up to 20%), and different types of aerosol particles prevail during summer (Yang et al., 2021), making it an ideal region for the study of the aerosol effect on shallow precipitation. Using the combined data set of GPM DPR

and MERRA-2 (Modern-Era retrospective analysis for Research and Applications, Versions2), this study aims to answer the following questions: 1) Do coarse and fine aerosol particles enhance or diminish the surface precipitation associated with shallow precipitation? 2) In what manner do aerosol particles influence the microphysical structures or processes of precipitation (such as break-up and collision-coalescence)? 3) To what extent are the relationships between aerosol particles and rainfall, microphysical structures, and processes sensitive to the dynamical and vapor components? The data and methods are introduced in Section 2. Section 3 discusses the impacts of fine and coarse aerosol particles on the microphysical properties and processes for shallow precipitation. A summary and conclusions are presented in Section 4.

2 Data and Methods

2.1 Data

In this study, four different data set are used to illustrate the potential impact of aerosol particles on microphysical precipitation structures and shallow precipitation processes over southern China during the summers between 2014 and 2021.

In the present study, the hourly MERRA-2 aerosol dataset (MERRA2_400.tavg1_2d_aer_Nx) at 0.5 × 0.625 spatial resolution is used, which has been widely utilized with the advantage of high temporal and spatial resolution. MERRA-2 is produced using the Goddard Earth Observing System, Version 5 (GEOS-5) atmospheric model and the Gridpoint Statistical Interpolation (GSI) assimilation system (Molod et al., 2015). GEOS-5 integrates a radiatively coupled version of the Goddard Chemical Aerosol Radiation and Transport (GOCART) model to simulate aerosol components (Chin et al., 2002). In the estimation of aerosol properties, MERRA-2 assimilates aerosol data from ground-based observations from the Aerosol Robotic NETwork (AERONET) and spaceborne aerosol products from the Advanced

Very High Resolution Radiometer (AVHRR), Multiangle Imaging Spectro Radiometer (MISR) (Randles et al., 2017; Buchard et al., 2017). Previous studies have shown a relatively good consistency of aerosol optical depth (AOD) from MERRA-2 and ground-based observations, i.e., AERONET, Sun sky radiometer Observation NETwork (SONET) (Ou et al., 2022; Buchard et al., 2015; Sun et al., 2019a). The correlation coefficient between MERRA-2 AOD and AERONET could reach 0.92 in summer China (Sun et al., 2019a). However, there is a slight underestimation of MERRA-2 AOD when compared to situ observations. Ou et al. (2022) revealed that the MERRA-2 AOD is underestimated by approximately 0.1 compared to a SONET station over South China. This is mainly because MERRA-2 lacks nitrate aerosol particles, leading to underestimations in the estimation of total AOD and fine aerosol particles (Sun et al., 2019b; Ou et al., 2022). The fine and coarse aerosol-polluted environment is defined by not only the AOD thresholds but also the AOD fractions to the total AOD, which may reduce uncertainties caused by underestimating AOD to some extent.

Aerosol species, including black carbon, organic carbon, sulfate, sea salt, and dust, are assumed to be external mixtures that do not interact with each other. In the present study, we consider the aerosol optical thickness and the extinction at 550 nm for five species, i.e. black carbon, organic carbon, sulfate, sea salt, and dust, as well as the Angstrom exponent (α) between 470 and 870 nm. α is a significant parameter in aerosol science, which elucidates the AOD dependency on wavelength. A higher α is related to a higher concentration of fine particles, whereas a lower α suggests a higher concentration of coarse particles (Lolli et al., 2023).

The GPM DPR consists of two precipitation radars operating in the Ka and Ku bands, providing a unique opportunity to obtain information on three-dimensional precipitation and particle drop size distributions (DSDs) at the same time. In the present study, the official DPR (version 7) dataset covering the summers (June to August) of 2014 and 2021 is also used, which provides information on the observation time, near-surface rain rate (RR), liquid water path (LWP), the three-dimensional profiles of attenuation-corrected reflectivity (Z_e), rainfall, the mass-weighted mean diameter D_m (in mm) and the generalized intercept N_w (i.e., number concentration of droplets in mm^{-}

^{1} m^{-3}) of the normalized gamma distributions with a vertical resolution of 125 m in each scanning pixel (Iguchi et al., 2017). The reliability of DSDs and precipitation has been validated by many previous studies (Huang et al., 2021; Radhakrishna et al., 2016). Due to the high spatial resolution (125 m in vertical and 4.5 km in horizontal resolution), the official 2ADPR (version 7) dataset has been widely used in the field of climatology (Chen et al., 2024; Zhang et al., 2020a; Chen et al., 2020). Shallow precipitation clouds are defined by their near-surface RR exceeding 0.1 mm h^{-1} and storm top height (STH) below 5 km in altitude. The STH is defined as the maximum height where the Z_e exceeds 20dBZ (Liu and Zipser, 2013).

In this study, convective available potential energy (CAPE) and relative humidity (RH) at 850 hPa from the fifth-generation global reanalysis of the European Center for Medium-Range Weather Forecasts (ERA5) covering the period from 2014 to 2021 are also used to investigate the meteorological dependence on the relationship between aerosol particles and precipitation. Additionally, the global 1km grid quality-controlled global digital elevation model (DEM) (https://ngdc.noaa.gov/mgg/topo/globe.html) is also used to exclude the influence of topography in the present study.

2.2 Methods

Due to the different spatial and temporal resolutions of DPR, MERRA-2, and ERA5, Prior to examining the potential influence of various aerosol types on shallow precipitation, it is necessary to harmonize these three datasets. Since the DPR detects the rainy pixels at approximately 4.5 km spatial resolution, both MERRA-2 at 0.5 × 0.625° resolution and ERA5 at 0.25° resolution are first linearly interpolated to 0.05° resolution. To accurately depict the aerosol conditions preceding shallow precipitation, observations of AOD from MERRA-2, corresponding closely to the timing of DPR observations and with a spatial resolution of 0.05°, are utilized. Concurrently, atmospheric data derived from ERA5 at a 0.05° resolution, which is in closest proximity to the center and observation time of the DPR pixel, are also used. The aerosol fine

mode AOD is defined as the total AOD sum of partial AOD of black carbon, organic carbon, and sulfate, while the AOD of coarse aerosol particles is the total value of the sum of AOD values of sea salt and dust particles (Gelaro et al., 2017). Additionally, to eliminate the potential impact of topography on precipitation and aerosol analysis, the study includes only shallow precipitation pixels that occur over regions with a topographic elevation of less than 100 meters.

Figure 1a illustrates the probability density of the joint distribution of AOD and α prior to the occurrence of shallow precipitation events. Shallow precipitation is most probable when the AOD is approximately 0.4 and α is approximately 1.4, which suggests a predominance of the fine aerosol mode. This can be primarily attributed to the increased presence of fine aerosol particles in South China during summer season, as represented in Figure 1b, where the probability density distributions (PDF) of AOD for fine aerosol particles and total aerosol particles reveal comparable values. Nonetheless, shallow precipitation is also evident in settings characterized by coarse aerosol particles, exhibiting a significant frequency when α is less than 1 and AOD is less than 0.3, as shown in Figure 1a.

There are three types of aerosol conditions discussed in the present study: clean environment, fine aerosol-polluted environment, and coarse aerosol-polluted environment. To classify clean and aerosol-polluted conditions over South China, PDFs of AOD for fine, coarse, and total aerosol particles are calculated before shallow precipitation, as shown in Figure 1b. It can be observed that the coarse mode AOD is relatively small, primarily distributed between 0 and 0.2, while fine mode AOD and total AOD are almost equal, mainly concentrated between 0 and 1.0. Specifically, the peak frequency occurs at an AOD of approximately 0.1 for coarse aerosol particles, 0.15 for fine aerosol particles, and 0.2 for total aerosol particles. We define a clean environment as one in which the AOD of the total aerosol particles falls below the 30th percentile in all the data sampled, specifically the AOD of the total aerosol particles < 0.225 (see Table 1 for reference). A fine (or coarse) aerosol-polluted environment must not only exceed 60% quantiles across all sampled data but also have the AOD of fine

(or coarse) particles exceeding 50% of the AOD for total aerosol particles. This approach ensures that in fine (or coarse) aerosol-polluted environments, fine (or coarse) particles are the primary influencing factor. Based on these standards, a coarse aerosol-polluted environment is classified as having a coarse AOD > 0.0425, as well as the proportion of coarse AOD to total aerosol particles exceeds 50%. Similarly, a fine aerosol-polluted environment is defined by a fine AOD > 0.315, with the proportion of fine AOD to total aerosol particles exceeding 50% (see Table 1 for reference). A sensitivity test was conducted with different thresholds to ensure the robustness of the present study. The results indicate that varying the thresholds does not significantly affect the conclusions of the work. During the study period, there are 9237, 9785, and 2566 shallow precipitation samples under clean, fine aerosol, and coarse aerosol-polluted conditions, respectively (Figure 1c). The mean AODs of five aerosol species under various environmental conditions are calculated to understand the contributions of different aerosol types (not shown). In South China, the primary contributors to aerosol species are sulfate aerosol particles, sulfate aerosol particles, and sea salt aerosol particles in clean, fine, and coarse aerosol-polluted environments, respectively. The shallow precipitation accounts for a higher proportion with respect to the total precipitation samples, reaching ~8% in clean and fine aerosol-polluted conditions (Figure 1c). However, under coarse aerosol-polluted conditions, the proportion of shallow precipitation samples is much lower, at around ~2%. Due to the lower AOD of coarse aerosol mode, occurrences, where the AOD of coarse aerosol particles accounts for more than 50% of the total AOD are less frequent, which explains the lower shallow precipitation samples in coarse aerosol-polluted conditions. However, the approximately 2500 samples ensure the reliability of our research results to some extent.

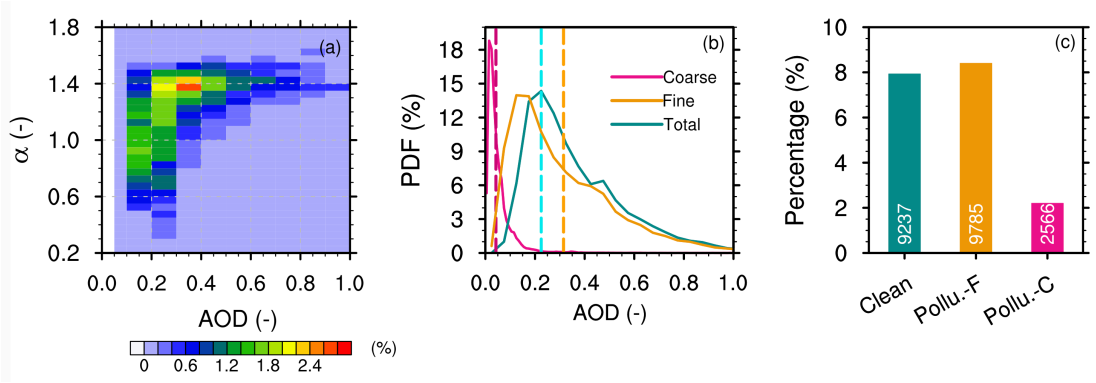

Figure 1 The observed frequency of AOD and α prior to the occurrence of shallow precipitation is illustrated in (a). The probability distribution functions of AOD for fine, coarse, and total aerosol particles before shallow precipitation events are depicted in (b). The proportion of shallow precipitation samples relative to total precipitation samples, categorized by different aerosol particle conditions, is shown in (c), as recorded by DPR in southern China during the summers from 2014 to 2021. The pink vertical line (orange) in (b) represents the upper 60% threshold for fine (coarse) aerosol particles, respectively. The cyan vertical line in (b) denotes the lower 30% threshold for the total AOD. The shallow precipitation samples are represented by white text in (c).

Table 1 Definitions of polluted and clean conditions of coarse and fine aerosol modes in southern China during the summers from 2014 to 2021.

Environment	Definition
Clean	Total AOD < 0.225
Polluted_Fine	Fine AOD > 0.315 & Fine AOD ratio>50%
Polluted_Coarse	Coarse AOD> 0.0425 & Coarse AOD ratio>50%

3 Results

3.1 Influence of aerosol particles on rainfall and microphysical characteristics

Figure 2 exhibits boxplots illustrating the near-surface RR, N_w, D_m, and Z_e at an

altitude of 2.5 km, alongside LWP and STH, for shallow precipitation under varying aerosol conditions in South China. Compared to clean environment, the RR decreases slightly during fine aerosol-polluted conditions, with a median value of only 0.7 mm h^{-1}, while in presence of coarse mode aerosol-polluted environment, the median value of RR increases, reaching 1.0 mm h^{-1}. This is consistent with a higher median Z_e at 2.5 km in altitude (25 dBZ) under coarse aerosol-polluted conditions and a lower one (22 dBZ) under fine aerosol-polluted conditions, suggesting the inhibition effect of fine particles and the invigoration effect of coarse particles on the near-surface RR for shallow precipitation. Nevertheless, the presence of coarse aerosol-polluted conditions appears to inhibit the vertical development of shallow precipitation clouds (Figure 2f), with a significantly lower median STH (~3.2 km) than that (~3.7 km) for fine aerosol-polluted environments. Examining the situation from a microphysical standpoint, it is observed that in comparison to a clean environment, there is a reduction in the median values of LWP at approximately 170 g m^{-2}, N_w at 34, and D_m at 1.05 mm at an altitude of 2.5 km in fine mode aerosol environments. On the contrary, under coarse aerosol-polluted conditions, the median values of LWP, N_w, and D_m at 2.5 km altitude increase, reaching 210 g m^{-2}, 35, and 1.15 mm, respectively. This indicates that the enhancement of near-surface RR under coarse aerosol-polluted conditions is contributed by higher concentrations of large rain droplets, while the weakening under fine aerosol-polluted conditions is influenced by lower concentrations of small rain droplets. In South China, sea salt aerosol particles are the primary components of coarse particles, and a recent study by Liu et al. (2022) has shown that sea salt aerosol particles are more likely to form large cloud droplets through hygroscopic growth, facilitating the formation of raindrops through condensation within shallow precipitation clouds. On the contrary, fine aerosol particles tend to reduce the effective radius of cloud droplets, with small cloud droplets being prone to evaporation and subsequent loss of cloud water. Our results fill the gap between cloud microphysics, precipitation microphysics, and rainfall.

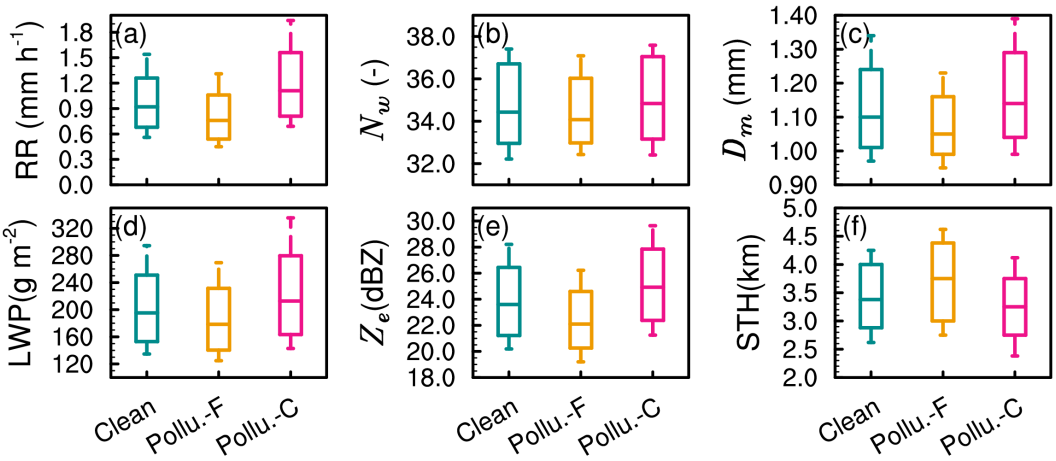

Figure 2 The box plot presents the near-surface rain rate (a), N_w (b), D_m (c), LWP (d), Z_e (e), and STH (f) for shallow precipitation across varying aerosol conditions in southern China during the summer seasons from 2014 to 2021. The top and bottom edges of the boxes indicate the upper and lower tritile, respectively. The line inside the box denotes the median. The whiskers extending from the box illustrate the upper and lower quartiles.

DSDs directly impact RR. Therefore, the DSDs at 2.5 km altitude for shallow precipitation clouds over southern China under three aerosol particle conditions are illustrated in Figure 3. Irrespective of the aerosol particle background, the DSDs are characterized by a high concentration of small droplets and a low concentration of large droplets, aligning with prior research findings (Wang et al., 2016; Chen et al., 2022). In a clean environment (Figure 3a), the DSD of shallow precipitation exhibits a high-frequency center around N_w of approximately 40, with D_m around 1.0 mm, reaching a frequency exceeding 70%. A secondary peak (40%) slightly shifts towards the lower right, located at D_m around 1.2 mm and N_w around 32. In the case of fine aerosol-polluted environments (Figure 3b), the average RR (1.15 mm h^{-1}) and D_m (1.14 mm) are slightly reduced compared to the clean environment, while the mean N_w increases slightly to 36.37. Furthermore, the secondary peak observed in a clean environment becomes more pronounced under fine aerosol-polluted conditions, with a frequency exceeding 50%. In contrast to clean and fine aerosol-polluted environments, both the mean values of RR and N_w increase under coarse aerosol-polluted conditions (Figure

3c). Furthermore, the DSD reveals more samples with D_m exceeding 2 mm or N_w exceeding 40, further indicating the enhancement of RR for shallow precipitation in coarse aerosol-polluted environments.

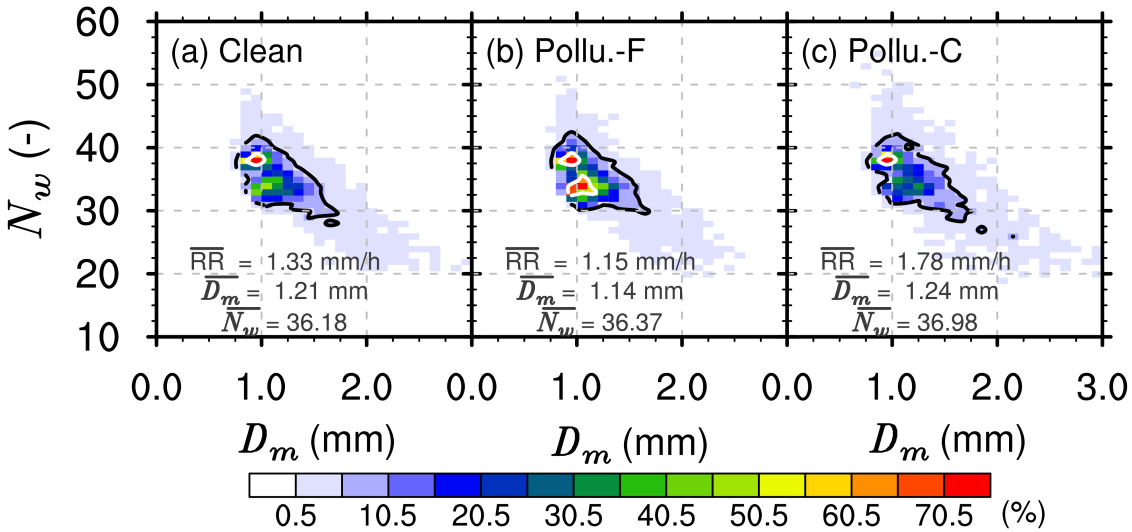

Figure 3 DSDs at 2.5 km altitude for shallow precipitation in clean (a), fine (b) and coarse (c) aerosol-polluted environments over southern China during the summers from 2014 to 2021. The mean values of D_m and N_w under different aerosol particle conditions are presented in each panel. The 5% and 50% contours are indicated by black and white solid lines, respectively.

3.2 Influence of aerosol particles on microphysical structures and processes

The above analysis has shown significant differences in near-surface RR and DSD for shallow precipitation under different aerosol particle environments. The vertical structure of precipitating clouds is closely related to near-surface RR and DSD, reflecting the thermal and dynamic structure within the clouds. Investigating the precipitation and microphysical structures under different aerosol particle backgrounds can further deepen our understanding of the thermodynamic and microphysical mechanisms by which aerosol particles affect shallow precipitation near the surface.

Figure 4 presents the profiles of the median values of Z_e, RR, D_m, and N_w for shallow precipitation over southern China in summer in three different types of aerosol particle environments. In general, shallow precipitation exhibits an increase in Z_e, RR, D_m, and N_w with a decrease in altitude across various aerosol particle environments, suggesting that the growth process of shallow precipitation is predominantly governed by warm rain collision-coalescence mechanisms. This is similar to the precipitation structures for shallow precipitation in the Yangtze-Huaihe River Basin (Chen et al., 2024). However, the median values of Z_e, RR, D_m, and N_w at each altitude differ under different types of aerosol particle environments. The promotion effect of coarse aerosol particles and the inhibition effect of fine aerosol particles are present throughout the profile. For example, the median values of Z_e, RR, D_m, and N_w at any given altitude are the largest in a coarse aerosol-polluted environment and the smallest in a fine aerosol-polluted pollution. Furthermore, the most significant differences in precipitation microphysical structures under different aerosol backgrounds occur near the surface (below 2 km). For example, at 1 km altitude, the differences in Z_e, RR, D_m, and N_w are approximately 3 dBZ, 0.4 mm h^{-1}, 0.12 mm and 1, respectively.

Considering the increasing amplitude of the median values of Z_e, RR, D_m, and N_w with decreasing altitude, there are significant differences under different aerosol backgrounds, reflecting different microphysical precipitation processes within shallow precipitation systems. Specifically, in coarse aerosol-polluted environments, the growth rates in Z_e, RR, D_m, and N_w from the 3 km to 1 km altitude layer are the largest, while these growth rates are the lowest in fine aerosol-polluted environments. This explains why a concentration increase of coarse particles results in an enhancement of RR compared to a clean environment, whereas an increase in fine aerosol particles leads to a precipitation suppression. For instance, the median D_m in pristine environments shows an increment from 1.07 mm at 3 km altitude to 1.1 mm at 1 km. In environments polluted by coarse aerosol particles, D_m exhibits a more pronounced increasing trend, with the median D_m rising from 1.08 mm at 3 km to 1.14 mm at 1 km. Conversely, with fine aerosol particles, the change in the median D_m from 3 km to 1 km is negligible, almost remaining constant at approximately 1.04 mm.

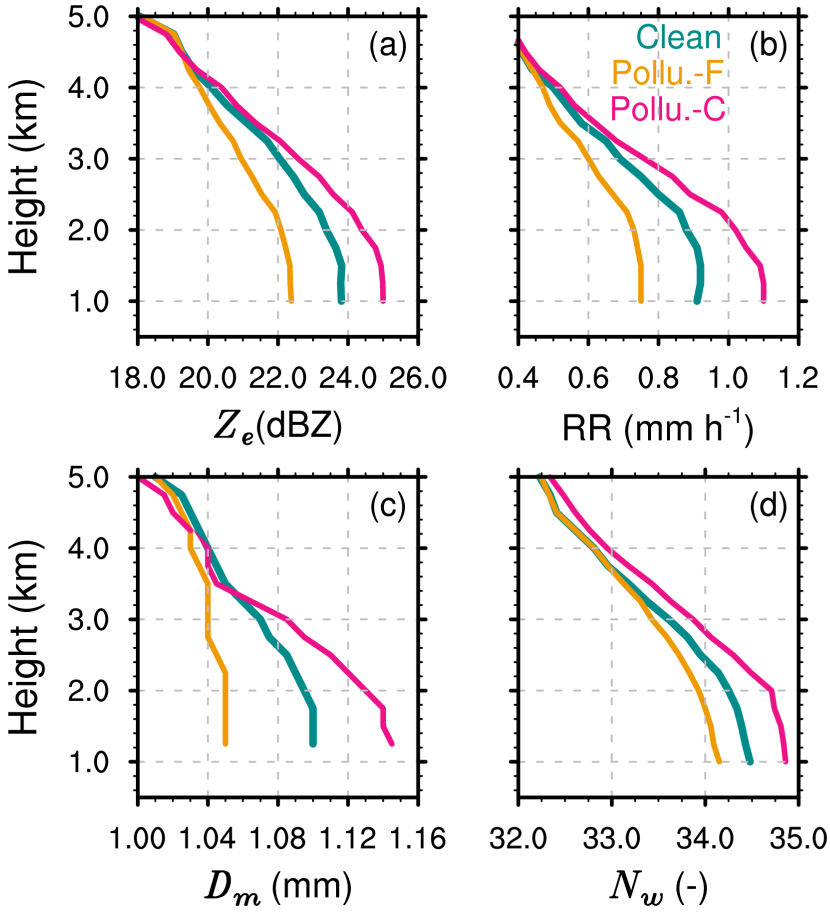

Figure 4 The profiles of the median Z_e (a), rain rate (b), D_m (c), and N_w (d) for shallow precipitation in different aerosol particle conditions over southern China during the summers from 2014 to 2021.

To more intuitively reflect the potential impact of different types of aerosol particles on the near-surface microphysical processes of shallow precipitation, the methods of Kumjian et al. (2014) are adopted to quantify the near-surface microphysical processes using changes in Z_e ($\Delta Z_e = Z_e^{1km} - Z_e^{3km}$) and D_m ($\Delta D_m = D_m^{1km} - D_m^{3km}$) at 3 km and 1 km. For example, collision-coalescence typically causes increases in Z_e and D_m, while breakup causes decreases. Similarly, an upward trend in D_m combined with a downward trend in Z_e as they approach the ground (positive ΔD_m and negative ΔZ_e) indicates evaporation or size sorting is the dominant process. The

signature of a "balance" between collision-coalescence and breakup is shown by a minor reduction in D_m and a rise in Z_e.

Figure 5 shows the proportions of collision-coalescence, size sorting, breakup, and balance processes of raindrops in shallow precipitation clouds under three different aerosol backgrounds. In general, the microphysical process of collision-coalescence of raindrops dominates shallow precipitation, accounting for more than 60%. This is followed by the raindrop breakup process, which accounts for more than 20%, while size sorting and balance processes account for the smallest proportions, only about 3% and 1%, respectively. In presence of fine aerosol-mode, the proportion of the collision-coalescence process is only 62.4%, while this proportion reaches 74.1% in coarse aerosol-polluted environments, with an increase of about 11.7%. Similarly, the proportion of the raindrop breakup process is 33.1% , with a decrease of 10% compared to 22.1% in coarse aerosol-polluted environments. This indicates the increase in the proportion of raindrop breakup processes and the weakening of the collision-coalescence process in fine aerosol-polluted environments, which may be the reason for the weakened near-surface RR. Conversely, in coarse aerosol-polluted mode environments, raindrops undergo more collision-coalescence growth processes and fewer breakup and evaporation processes, which contributes to the enhancement of surface RR.

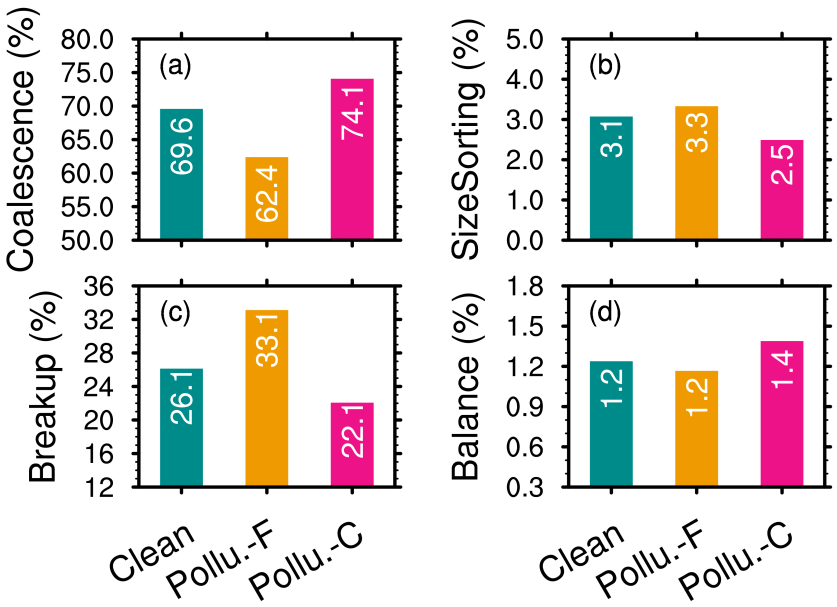

394

395 **Figure 5** The percentages of coalescence (a), size sorting (b), break up(c), and
396 balance (d) for shallow precipitation shallow precipitation raindrops under different
397 aerosol particle conditions in southern China during the summers from 2014 to 2021.
398

399 ***3.3 Sensitivities of aerosol impacts on precipitation to meteorological factors***

400 The findings from the prior section demonstrate that shallow precipitation shows
401 notable variations in surface RR, precipitation structures, and microphysical processes
402 depending on different aerosol particle conditions. However, precipitation itself is a
403 complex process influenced by multiple thermal and dynamic environmental factors,
404 such as instability, humidity, temperature, and wind vectors. Among these, dynamic
405 conditions and moisture levels are particularly important indicators. Therefore, CAPE
406 and RH at 850 hPa, which, respectively, reflect atmospheric instability and moisture,
407 are used to isolate and assess the impact of aerosol particles. CAPE is divided into three
408 intervals based on the terciles of CAPE values during precipitation events in southern
409 China: CAPE 333 J kg^{-1} (CAPE1), 333 < CAPE < 1031 J kg^{-1} (CAPE2), and CAPE
410 1031 J kg^{-1} (CAPE3). Similarly, RH at 850 hPa is divided into three intervals, that is,
411 RH 83% (RH1), 83% < RH < 91% (RH2), and RH 91% (RH3).

The box plots of RR, LWP, and STH, as well as N_w, D_m, and Z_e at 2.5 km altitude for shallow precipitation in southern China under different aerosol particle backgrounds and CAPEs are presented in Figure 6. Consistent with the conclusions of Figure 2, it becomes apparent that under varying CAPE conditions, the median STH of shallow precipitation clouds attains its lowest values in coarse aerosol-polluted environments, whereas the median RR and Z_e at an altitude of 2.5 km reach their highest levels. On the contrary, the median STH is the highest, but the median RR and Z_e at 2.5 km are the lowest in a fine aerosol-polluted environment. This indicates that the suppression of RR in fine aerosol-polluted environments and the invigoration of RR in coarse aerosol-polluted environments are independent of the dynamic conditions (CAPE in this case). Furthermore, when seen from microphysics, under different CAPE conditions, shallow precipitation clouds in coarse aerosol-polluted environments exhibit the highest median values of values of LWP, N_w, and D_m at 2.5 km, while these variables are the lowest in fine aerosol-polluted environments. This helps explain why shallow precipitation has the highest near-surface RR in coarse aerosol-polluted environments and the lowest surface RR in fine aerosol-polluted environments from the microphysical perspective.

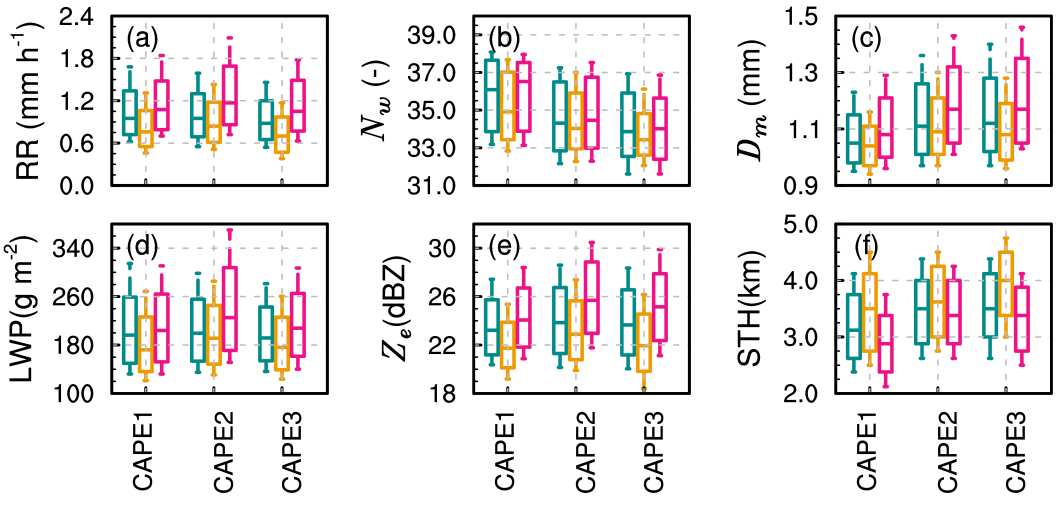

Figure 6 Box plot of the near-surface rain rate (a), N_w (b), D_m (c), LWP (d), Z_e (e), and STH (f) under different aerosol particle and CAPE conditions for shallow precipitation over southern China during the summers of 2014-2021. The blue, orange

and pink colors indicate the clean, fine-aerosol polluted and coarse-aerosol polluted environments, respectively. The boxes' top and bottom edges indicate the upper and lower tritile, respectively. The median is depicted by the line inside the box. The whiskers extending from the box illustrate the lower and upper quartiles.

Similarly, the sensitivity of humidity to the impact of aerosol particles on shallow precipitation is examined by presenting the box plots of precipitation parameters, as illustrated in Figure 7. Regardless of 850hPa-RH, the vertical development of shallow precipitation clouds is hindered in coarse aerosol-polluted environments, with the median STH being the smallest. However, the near-surface RR is the highest, corresponding to the highest median Z_e at 2.5 km. On the contrary, in fine particle pollution environments, the vertical development of shallow precipitation clouds is enhanced (with the highest median STH), but the near-surface RR and Z_e are the weakest. This further confirms that the impact of coarse and fine aerosol particles on near-surface RR and LWP is independent of moisture and dynamic conditions.

It is important to note that the degree of enhancement or suppression of RR by coarse and fine aerosol particles varies under different humidity conditions. Compared to high-humidity environments, coarse aerosol particles have the most significant enhancement effect on RR, while fine aerosol particles have the most significant suppression effect in relatively low-humidity environments (RH1). In fine aerosol-polluted environments, the box plot of RR shows a significant decrease compared to that in clean environments, while that in coarse aerosol-polluted environments shows a significant increase. Specifically, the median RR in the coarse aerosol-polluted environment is around 1.1 mm h^{-1}, while it is around 0.7 mm h-1 in the fine aerosol-polluted environment.

Regarding STH, under low relative humidity and fine aerosol-polluted conditions, shallow precipitation clouds develop more deeply, with the 25th percentile of STH reaching 5 km, significantly higher than in clean and coarse aerosol-polluted environments. This may be because there is a reduction in the effective radius of cloud droplets in fine aerosol-polluted and low-humidity conditions. Smaller cloud droplets

are more prone to evaporation, resulting in a lower LWP, which does not favor an increase in near-surface RR. This is also reflected in the near-surface DSD, which is characterized by lower N_w and smaller D_m. However, although the humidity is relatively low, the coarse particles, being more hygroscopic, can form larger cloud droplets, reducing the loss of cloud water due to evaporation (resulting in a higher LWP), and thereby enhancing surface RR. This is also reflected in the near-surface DSD, which is characterized by a higher N_w and larger D_m. In high humidity environments, a high concentration of fine particles can promote the formation of more cloud condensation nuclei, which to some extent reduces the loss of cloud water due to the evaporation of small particles. Therefore, the LWP in fine-particle pollution environments does not differ much from that in coarse aerosol-polluted environments. This may also lead to smaller differences in RR, Ze, and other variables between coarse and fine aerosol-polluted environments under relatively high humidity conditions.

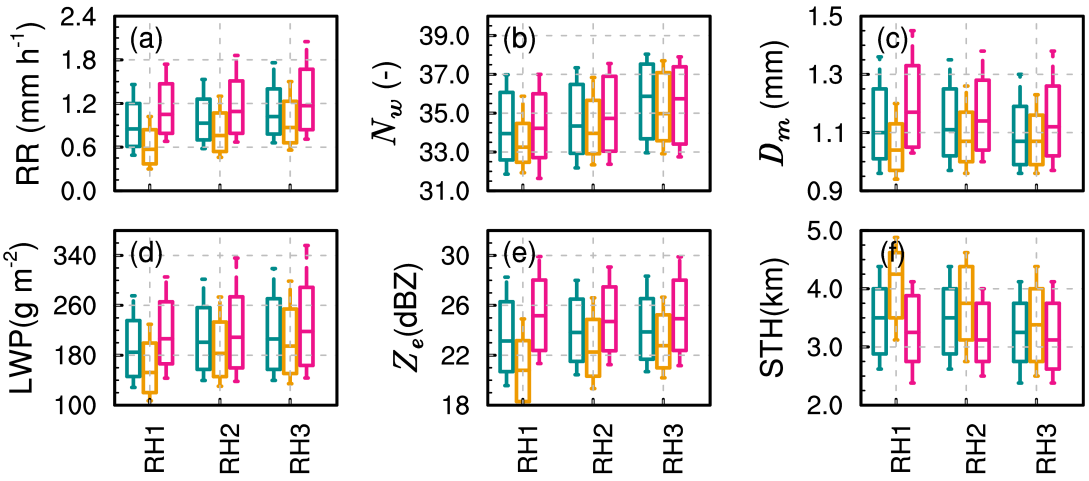

Figure 7 Same as Figure 6, but for RH at 850hPa. The blue, orange and pink colors indicate the clean, fine-aerosol polluted and coarse-aerosol polluted environments, respectively.

3.4 Sensitivities of aerosol impacts on microphysical structures and processes to meteorological factors

This part continues examining how coarse and fine aerosol modes affect precipitation structure and the microphysical processes in different environmental settings. As shown in Figure 8, under different CAPE and aerosol particle backgrounds, shallow precipitation profiles consistently exhibit increasing trends in Z_e, RR, N_w, and D_m with decreasing altitude. Furthermore, irrespective of CAPE values, at a specified altitude, the parameters Z_e and RR are observed to be at their maximum in environments polluted with coarse aerosol particles, followed by those in a clean environment, and at their minimum in environments polluted with fine aerosol particles. This is consistent with the results in Figure 4. When compared between different CAPE conditions, the Z_e, RR, and D_m of shallow precipitation in CAPE2 are the highest at different altitudes, while as the CAPE increases further (CAPE3), these values even decrease. Apart from instability, precipitation can be influenced by moisture, topography, and other factors; therefore, it is possible for an even lower RR in high CAPE conditions.

When seen from D_m and N_w (Figures 8c1-c3, d1-d3), the promotion effect of coarse aerosol particles and the suppression effect of fine aerosol particles can vary under different dynamic environmental conditions. Under moderate CAPE conditions (CAPE2), D_m and N_w in coarse aerosol-polluted environments are the largest at different altitudes, while D_m and N_w in a fine aerosol-polluted environment are the smallest. This indicates that under moderate CAPE conditions, the enhancement of RR in coarse aerosol-polluted environments is contributed by large particles and high concentrations. For low CAPE conditions (CAPE1), the median D_m above 3 km is even the smallest in coarse aerosol-polluted environments, compared to clean and fine aerosol-polluted environments. Therefore, the maximum values of RR and Z_e at this layer are mainly contributed by high concentrations of raindrops (with large median N_w, as shown in Figure 8d-1). For high CAPE conditions (CAPE3), the median N_w above the 3 km altitude layer in coarse aerosol-polluted environments is even the smallest. Therefore, the maximum values of RR and Z_e at this altitude are mainly contributed by high

concentrations of raindrops (with large median D_m, as shown in Figure 8c-3).

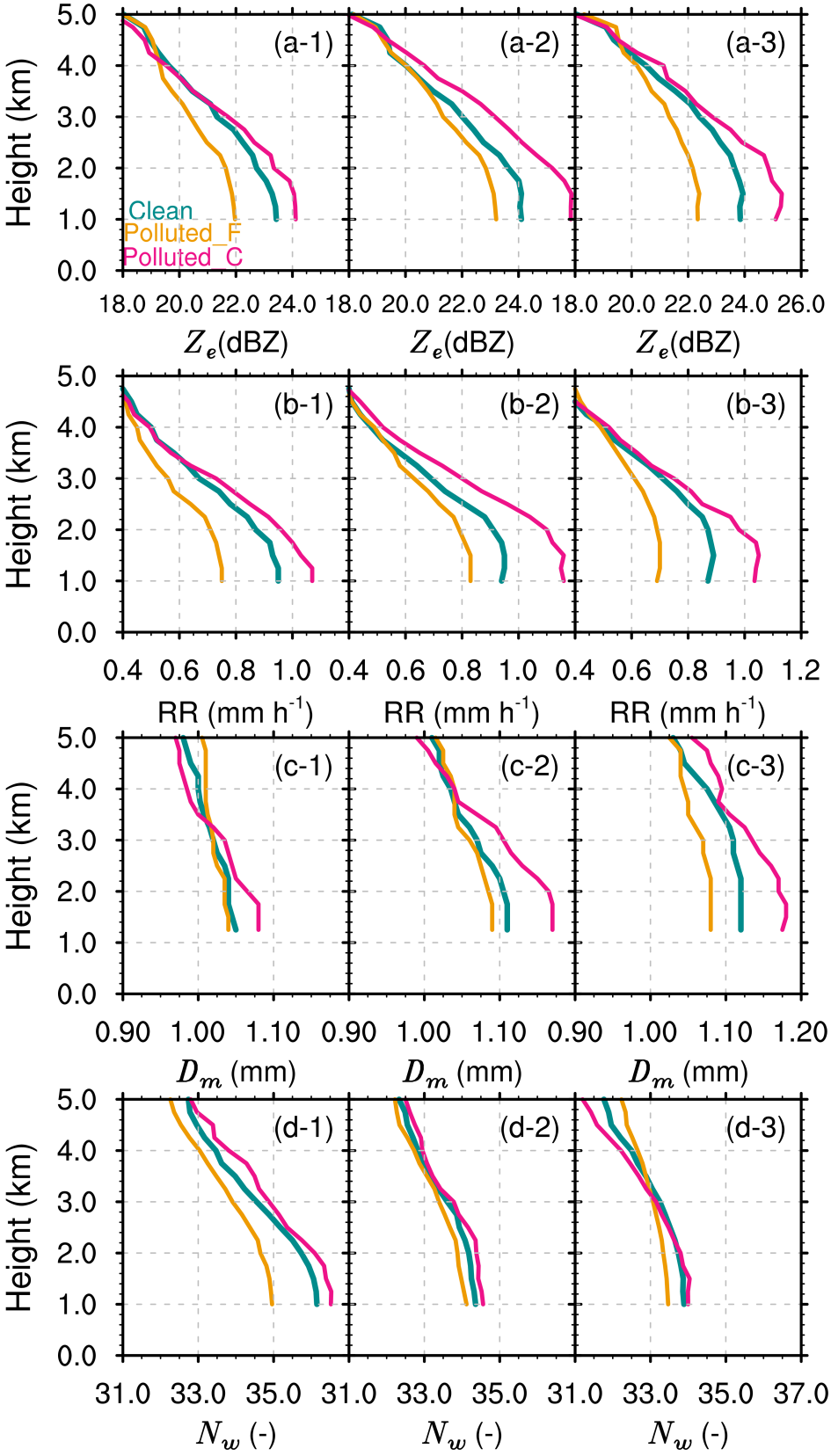

Figure 8 The Z_e (a), rain rate (b), D_m (c), and N_w (d) profiles for shallow precipitation in different aerosol particle and CAPE conditions over southern China during the summers from 2014 to 2021. CAPE1, CAPE2, and CAPE3 are shown in the left, middle, and right panels, respectively.

Similarly, the profiles of Z_e, RR, D_m, and N_w in different 850hPa-RH and aerosol particle backgrounds are illustrated in Figure 9. Consistent with previous research results, the median values of Z_e, RR, D_m, and N_w of shallow precipitation exhibit a gradual increase with decreasing altitude, reflecting the warm rain collision-coalescence growth process. However, the microphysical structures of shallow precipitation vary under different RH conditions with similar aerosol particle backgrounds. As RH at 850hPa increases, the median values of Z_e, RR, D_m, and N_w of shallow precipitation increase more significantly with decreasing altitude. For example, under low humidity conditions (RH1), the median D_m increases slightly when raindrops fall from 3 km to 1 km (Figure 9c-1), and even decreases under fine aerosol-polluted conditions, indicating more breakup processes. Subsequently, with increasing humidity, the increase in D_m becomes more apparent (Figure 9c-3). For example, the median D_m increases from 1.05 mm to 1.15 mm in coarse aerosol-polluted environments.

The median values of Z_e and RR across various aerosol particle backgrounds are markedly elevated in environments contaminated with coarse aerosol particles across all altitude layers, demonstrating a notable increase with decreasing altitude. Conversely, in conditions contaminated by fine aerosol particles, the median values of Z_e and RR are at their lowest at each altitude layer, exhibiting minimal increases as altitude decreases. This is consistent with previous conclusions (Figures 4 and 8), further indicating that the impact of coarse and fine aerosol particles on the near-surface RR and the precipitation structure is not sensitive to dynamic and moisture conditions. However, from a microphysical structure perspective, there are still some differences in aerosol particle backgrounds. Under low and moderate humidity conditions (RH1 and RH2), at a given altitude, D_m and N_w are the largest in coarse aerosol-polluted environments and the smallest in fine aerosol-polluted environments. In RH3 conditions at the same altitude, a clean environment has the highest N_w and a relatively small D_m; for coarse mode, N_w is moderate with the largest D_m; and for fine mdoe, N_w is the lowest with a relatively small D_m. This indicates that in high RH environments,

fine aerosol particles mainly reduce RR by suppressing the concentration of raindrops, while coarse aerosol particles increase RR by increasing the size of raindrops. Furthermore, the differences in precipitation structures in aerosol-polluted coarse and fine environments depend on humidity conditions, consistent with the conclusions in Figure 7. The differences are the greatest under RH1 conditions, with the differences in RR, Z_e, D_m, and N_w at 1 km altitude being 0.42 mm h^{-1}, 4.5 dBZ, 0.19 mm, and about 1.3, respectively. Under RH3 conditions, the differences are smallest, with the differences in the aforementioned variables being 0.35 mm h^{-1}, 2 dBZ, 0.05 mm, and approximately 0.8, respectively.

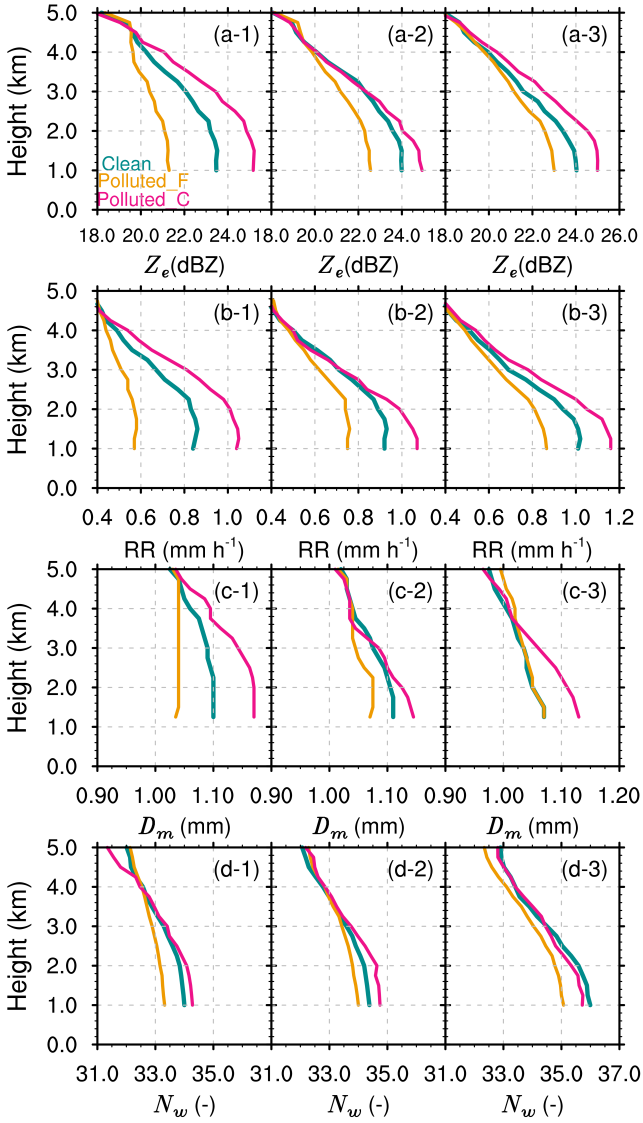

Figure 9 The Z_e (a), rain rate (b), D_m (c), and N_w (d) profiles for shallow precipitation in different aerosol particle conditions and 850 hPa-RH over southern China during the

summers from 2014 to 2021. RH1, RH2, and RH3 are shown in left, middle, and right panels, respectively.

To quantitatively analyze the dependence of microphysical processes on dynamics and moisture under different aerosol particle backgrounds, we examined the differences in the two primary microphysical processes, i.e., collision-coalescence and breakup. As a result of the low proportions of size sorting and balance, further analysis of these microphysical processes is not included. The microphysical processes of precipitation depend on the dynamic and moisture conditions. For instance, with decreasing CAPE and increasing RH, the proportion of collision-coalescence increases, while the proportion of breakup decreases in clean, coarse, and fine aerosol-polluted environments. Environments with high RH and low CAPE encourage aerosol particles in the boundary layer to gather moisture, leading to the formation of additional cloud droplets. These droplets then condense further to create more raindrops, thus enhancing the collision-coalescence process.

After comparing various aerosol particle backgrounds, it is possible to determine certain overarching patterns that remain consistent regardless of thermodynamic conditions. Initially, irrespective of CAPE, RH, or aerosol particle background, shallow precipitation systems predominantly exhibit the warm rain collision-coalescence process, with its occurrence proportion spanning from a minimum of 51.2% to a maximum of 82.3%.There is also a certain proportion of break-up processes, ranging from 14.6% to 43.2%. Second, regardless of the value of CAPE and RH, the proportion of the collision-coalescence process is always the highest in coarse aerosol-polluted environments, while the proportion of the breakup process is always the highest in fine aerosol-polluted environments. These conclusions are consistent with the results in Figure 5. However, the increase in the proportion of collision coalescence in coarse aerosol-polluted environments and the increase in the proportion of breakup in fine aerosol-polluted environments depend on dynamic and moisture conditions. For example, under low relative humidity (RH1) conditions, the proportion of the collision-coalescence process in coarse aerosol-polluted environments (73.4%) is significantly higher than that in fine aerosol-polluted environments (51.2%), with an enhancement of 22.2%. On the contrary, the proportion of the breakup process in fine aerosol-polluted environments (43.2%) is significantly higher than in coarse aerosol-polluted environments (22.3%). This is consistent with previous findings that under RH1

conditions, D_m in fine aerosol-polluted environments rapidly decreases with decreasing altitude.

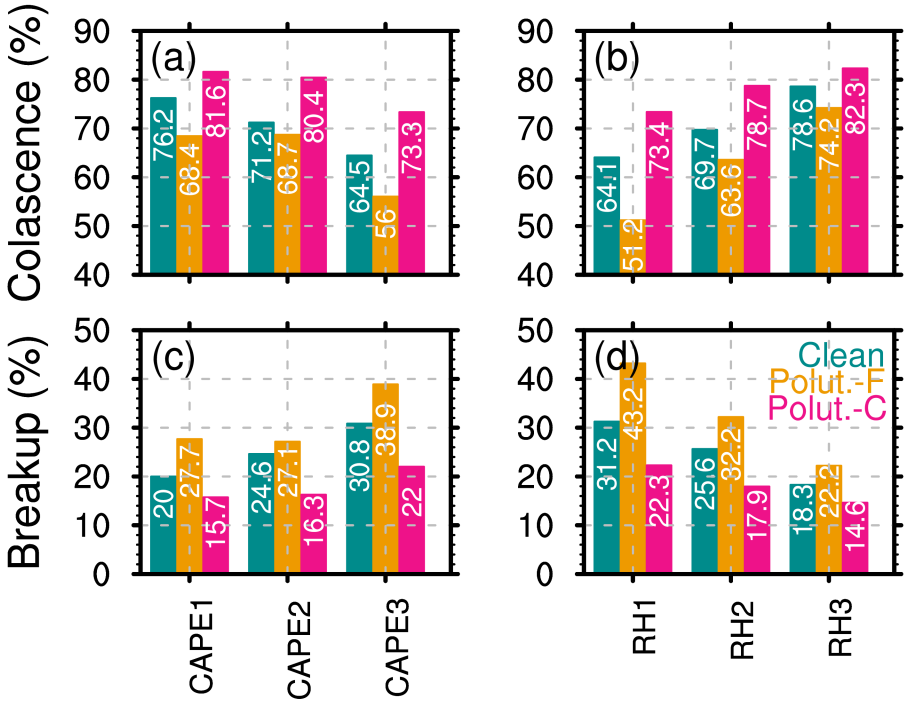

Figure 10 The percentages of coalescence (a, b) and break-up (c,d) for shallow precipitation raindrops under different aerosol particle, CAPE and 850 hPa-RH conditions in southern China during the summers from 2014 to 2021.

4 Conclusion and Discussion

Using the combined data of DPR, MERRA-2 aerosol datasets, and ERA5 during the summers of 2014-2021, this study investigates the potential impacts of coarse and fine aerosol particles on the Rain Rate (RR), microphysical structure, and processes for shallow precipitation in South China. Clean, coarse, and fine aerosol-polluted modes are classified according to the AOD for total aerosol particles, coarse aerosol particles, and fine aerosol particles derived from MERRA-2 products. ERA5 reanalysis data are used to explore the sensitivity of aerosol impacts on shallow precipitation to dynamic and moisture conditions in South China. The main findings are summarized as follows. In comparison to clean environments, coarse aerosol-polluted environments enhance

near-surface rainfall rates of shallow precipitation, characterized by stronger near-surface RR (average precipitation intensity of 1.78 mm h^{-1}), higher concentrations (average N_w = 36.98) of raindrops at larger sizes (average D_m = 1.24 mm). This can be ascribed to the high presence of sea salt aerosol particles in South China, which tend to form larger cloud droplets through hygroscopic growth. This, in turn, enhances the condensation process, leading to the formation of additional rain droplets. As a result, it facilitates the coalescence and growth of raindrops, ultimately contributing to the formation of larger raindrops. On the contrary, fine aerosol particles suppress near-surface RR, with an average near-surface RR of only 1.33 mm h^{-1} and lower concentrations and smaller sizes of raindrops (average N_w = 36.37, average D_m = 1.14 mm). Liu et al. (2022) noted similar opposing effects of fine aerosol particles and coarse sea spray on warm marine clouds. Deep clouds show increased rainfall with high liquid water content but reduced rainfall if water content is low (Li et al., 2011). This underscores the distinct behavior of shallow precipitation and the varied impacts of aerosol types on it. However, fine aerosol-polluted environments promote vertical development of shallow precipitation clouds (median STH of 3.7 km), approximately 0.5 km higher than in coarse aerosol-polluted conditions. The inhibition of the vertical development of precipitation clouds by coarse aerosol particles explains their suppressive effect on lightning activity to some extent (Pan et al., 2022).

From the perspective of precipitation vertical structure and microphysical processes, shallow precipitation is dominated by warm-rain collision-coalescence processes under different aerosol particle backgrounds, with the collision-coalescence process accounting for over 62%. However, there are significant differences in the efficiency of raindrop collision-coalescence growth under different aerosol particle conditions. In contrast to clean conditions, the median values of Z_e, RR, D_m, and N_w are highest in presence of aerosol coarse mode and lowest in conditions for fine aerosol mode at all altitude levels. Looking at it from a microphysical standpoint, the increase in D_m with decreasing altitude is most pronounced under coarse aerosol-polluted conditions, reflecting more significant collision-coalescence growth processes, accounting for 74.1%. In contrast, the increase in D_m with decreasing altitude is weakest

under fine aerosol-polluted conditions, due to the higher proportion of breakup processes (accounting for 33.1%) and a decrease of approximately 12% in the collision-coalescence process (accounting for 62.4%). Overall, the promotion of RR is associated with more significant collision-coalescence processes by coarse aerosol particles, while the suppression of RR is characterized by more significant breakup processes with fine aerosol particles.

The effects of fine and coarse aerosol particles on the suppression and enhancement of RR are independent of CAPE and humidity, consistent with the findings by Liu et al. (2022). However, our results show that the extent of suppression or enhancement varies with CAPE and humidity. Additionally, the analysis of aerosol-precipitation interactions under different surface air temperatures yields results similar to those observed for CAPE and RH at 850 hPa (figures not shown). The promotion and suppression effects are the most pronounced under low relative humidity conditions (RH1). This is mainly contributed by the stronger suppression of fine aerosol particles in low-humidity environments. For instance, the median RR is around 1.12 mm h^{-1} under coarse aerosol-polluted conditions, while it is around 0.7 mm h^{-1} under fine aerosol-polluted conditions, with a difference of approximately 0.42 mm h^{-1}. The collision-coalescence and breakup microphysical processes play an important role in these differences, with the collision-coalescence accounting for 73.4% under coarse aerosol-polluted conditions, which is 22.2% higher than the 51.2% observed under fine aerosol-polluted conditions. Correspondingly, the breakup microphysical processes account for 43.2% under fine aerosol-polluted conditions, significantly higher than the 22.3% in coarse aerosol-polluted conditions. Under high relative humidity conditions, fine aerosol-polluted environments primarily reduce RR by inhibiting raindrops concentration (possibly as a result of the evaporation effects of small cloud droplets), while coarse aerosol particles invigorate RR by increasing the size of raindops. Additionally, the increase in RR above 3 km in coarse aerosol-polluted environments is mainly driven by the high concentration of hydrometeors in low instability conditions, while by large hydrometeors in high instability environments. It is important to note that precipitation is a complex process influenced by multiple meteorological factors,

including instability, moisture, and temperature. Additionally, other factors such as wind vectors and pressure may also affect the impact of aerosol particles on precipitation, which is worthy of further study.

This study primarily elucidates the microphysical processes within shallow precipitation systems under varying aerosol particle conditions. However, the methods and data utilized have broad application potential. Future research could extend these approaches to explore the relationship between deep convection or mixed-phase clouds and aerosol particles. Such investigations could reveal the complex effects of aerosol particles on the precipitation process and further enhance our scientific understanding of the physical connections between aerosol particles and precipitation microphysics. However, it is important to note that the spatial resolution of MERRA-2 and ERA5 is much coarser than that of DPR. The interpolation methods employed in the present study may introduce errors and may not fully capture the true conditions, making it challenging to accurately assess fine-scale processes in aerosol-cloud interactions. Furthermore, MERRA-2 shows a slight underestimation of approximately 0.1 compared to in-situ observations in South China (Ou et al., 2022), probably due to the absence of nitrate aerosol particles in the MERRA-2 dataset. Consequently, the fine aerosol-polluted environments examined in this study may not fully capture conditions with high nitrate loading. There is an urgent need for long-term observational data on aerosol concentrations with high spatiotemporal resolution and accuracy to fully capture the samples of high aerosol particles loading and more effectively capture fine-scale processes in aerosol-cloud interactions.

Data availability

The GPM DPR data provided by NASA Goddard Space Flight Center's Mesoscale Atmospheric Processes Laboratory and Precipitation Processing System (PPS) can be downloaded from https://pmm.nasa.gov/dataaccess/downloads/gpm. MERRA-2 data can be downloaded from https://gmao.gsfc.nasa.gov/reanalysis/MERRA-

2/data_access/. The ERA5 data can be downloaded from https://www.ecmef.int/en/forecasts/dataset/ecmwf-reanalysis-v5. The ancillary digital terrain data is from the National Geophysical Data Center (NGDC) (available online at http://www.ngdc.noaa.gov, accessed in May 2023).

Author contributions

YY designed the manuscript and led the data analysis; FC performed the analysis and wrote the manuscript draft; YL and LY collected the data; GL, LY, and SL reviewed and edited the manuscript; SL helped with the data analysis.

Declaration of competing interest

The authors declare no competing interests.

Acknowledgments

The authors thank NASA Goddard Space Flight Center's Mesoscale Atmospheric Processes Laboratory and PPS, NGDC, and ECMWF for providing the analysis data.

Financial support

This work has been jointly supported by the China National Natural Science Foundation (grant 41805023), the Jiangsu Meteorological Bureau General Project (KM202407), the Open Grants of China Meteorological Administration Radar Meteorology Key Laboratory (2024LRM-B06), the Open Project of KLME & CIC-FEMD (KLME202303), China Meteorological Administration "Application of quantum technology in meteorological detection" Youth Innovation Team Project (No.CMA2024QN11), and the Open Project of State Key Laboratory of Severe Weather (2024LASW-B11).

Reference

Buchard, V., da Silva, A. M., Colarco, P. R., Darmenov, A., Randles, C. A., Govindaraju, R., Torres, O., Campbell, J., and Spurr, R.: Using the OMI aerosol index and absorption aerosol optical depth to evaluate the NASA MERRA Aerosol Reanalysis, Atmos. Chem. Phys., 15, 5743-5760, 10.5194/acp-15-5743-2015, 2015.

Buchard, V., Randles, C. A., da Silva, A. M., Darmenov, A., Colarco, P. R., Govindaraju, R., Ferrare, R., Hair, J., Beyersdorf, A. J., Ziemba, L. D., and Yu, H.: The MERRA-2 Aerosol Reanalysis, 1980 Onward. Part II: Evaluation and Case Studies, Journal of Climate, 30, 6851-6872, https://doi.org/10.1175/JCLI-D-16-0613.1, 2017.

Chen, F., Zheng, X., Wen, H., and Yuan, Y.: Microphysics of Convective and Stratiform Precipitation during the Summer Monsoon Season over the Yangtze–Huaihe River Valley, China, Journal of Hydrometeorology, 23, 239-252, 2022.

Chen, F., Zheng, X., Yu, L., Wen, H., and Liu, Y.: Precipitation, microphysical and environmental characteristics for shallow and deep clouds over Yangtze-Huaihe River Basin, Atmospheric Research, 298, 107155, https://doi.org/10.1016/j.atmosres.2023.107155, 2024.

Chen, Y., Zhang, A., Zhang, Y., Cui, C., Wan, R., Wang, B., and Fu, Y.: A Heavy Precipitation Event in the Yangtze River Basin Led by an Eastward Moving Tibetan Plateau Cloud System in the Summer of 2016, Journal of Geophysical Research: Atmospheres, 125, e2020JD032429, https://doi.org/10.1029/2020JD032429, 2020.

Chin, M., Ginoux, P., Kinne, S., Torres, O., Holben, B. N., Duncan, B. N., Martin, R. V., Logan, J. A., Higurashi, A., and Nakajima, T.: Tropospheric Aerosol Optical Thickness from the GOCART Model and Comparisons with Satellite and Sun Photometer Measurements, Journal of the Atmospheric Sciences, 59, 461-483, https://doi.org/10.1175/1520-0469(2002)059<0461:TAOTFT>2.0.CO;2, 2002.

Christensen, M. W. and Stephens, G. L.: Microphysical and macrophysical responses of marine stratocumulus polluted by underlying ships: 2. Impacts of haze on precipitating clouds, Journal of Geophysical Research: Atmospheres, 117, https://doi.org/10.1029/2011JD017125, 2012.

Fan, C., Wang, M., Rosenfeld, D., Zhu, Y., Liu, J., and Chen, B.: Strong Precipitation Suppression by Aerosols in Marine Low Clouds, Geophysical Research Letters, 47, e2019GL086207, https://doi.org/10.1029/2019GL086207, 2020.

Fan, J., Rosenfeld, D., Zhang, Y., Giangrande, S. E., Li, Z., Machado, L. A. T., Martin, S. T., Yang, Y., Wang, J., Artaxo, P., Barbosa, H. M. J., Braga, R. C., Comstock, J. M., Feng, Z., Gao, W., Gomes, H. B., Mei, F., Pöhlker, C., Pöhlker, M. L., Pöschl, U., and de Souza, R. A. F.: Substantial convection and precipitation enhancements by ultrafine aerosol particles, Science, 359, 411-418, 10.1126/science.aan8461, 2018.

Gelaro, R., McCarty, W., Suárez, M. J., Todling, R., Molod, A., Takacs, L., Randles, C. A., Darmenov, A., Bosilovich, M. G., Reichle, R., Wargan, K., Coy, L., Cullather, R., Draper, C., Akella, S., Buchard, V., Conaty, A., da Silva, A. M., Gu, W., Kim, G.-K., Koster, R., Lucchesi, R., Merkova, D., Nielsen, J. E., Partyka, G., Pawson, S., Putman, W., Rienecker, M., Schubert, S. D., Sienkiewicz, M., and Zhao, B.: The Modern-Era Retrospective Analysis for Research and Applications, Version 2 (MERRA-2), Journal of Climate, 30, 5419-5454, https://doi.org/10.1175/JCLI-D-16-0758.1, 2017.

Guo, J., Su, T., Chen, D., Wang, J., Li, Z., Lv, Y., Guo, X., Liu, H., Cribb, M., and Zhai, P.: Declining

765 Summertime Local-Scale Precipitation Frequency Over China and the United States, 1981–2012:
766 The Disparate Roles of Aerosols, Geophysical Research Letters, 46, 13281-13289,
767 https://doi.org/10.1029/2019GL085442, 2019.
768 Huang, H., Zhao, K., Fu, P., Chen, H., Chen, G., and Zhang, Y.: Validation of Precipitation
769 Measurements From the Dual-Frequency Precipitation Radar Onboard the GPM Core
770 Observatory Using a Polarimetric Radar in South China, IEEE Transactions on Geoscience and
771 Remote Sensing, 1-16, 10.1109/TGRS.2021.3118601, 2021.
772 Iguchi, T., Seto, S., Meneghini, R., Yoshida, N., Awaka, J., and Kubota, T.: GPM/DPR level-2
773 algorithm theoretical basis document, NASA Goddard Space Flight Center, Greenbelt, MD, USA,
774 Tech. Rep, 2017.
775 Jiang, M., Li, Z., Wan, B., and Cribb, M.: Impact of aerosols on precipitation from deep convective
776 clouds in eastern China, Journal of Geophysical Research: Atmospheres, 121, 9607-9620,
777 https://doi.org/10.1002/2015JD024246, 2016.
778 Koren, I., Dagan, G., and Altaratz, O.: From aerosol-limited to invigoration of warm convective
779 clouds, Science, 344, 1143-1146, doi:10.1126/science.1252595, 2014.
780 Kumjian, M. R., Khain, A. P., Benmoshe, N., Ilotoviz, E., Ryzhkov, A. V., and Phillips, V. T. J.: The
781 Anatomy and Physics of ZDR Columns: Investigating a Polarimetric Radar Signature with a
782 Spectral Bin Microphysical Model, Journal of Applied Meteorology and Climatology, 53, 1820-
783 1843, 10.1175/JAMC-D-13-0354.1, 2014.
784 Lang, F., Huang, Y., Protat, A., Truong, S. C. H., Siems, S. T., and Manton, M. J.: Shallow
785 Convection and Precipitation Over the Southern Ocean: A Case Study During the CAPRICORN
786 2016 Field Campaign, Journal of Geophysical Research: Atmospheres, 126, e2020JD034088,
787 https://doi.org/10.1029/2020JD034088, 2021.
788 Li, Z., Niu, F., Fan, J., Liu, Y., Rosenfeld, D., and Ding, Y.: Long-term impacts of aerosols on the
789 vertical development of clouds and precipitation, Nature Geoscience, 4, 888-894,
790 10.1038/ngeo1313, 2011.
791 Liu, C. and Zipser, E.: Regional variation of morphology of organized convection in the tropics
792 and subtropics, Journal of Geophysical Research: Atmospheres, 118, 453-466,
793 https://doi.org/10.1029/2012JD018409, 2013.
794 Liu, F., Mao, F., Rosenfeld, D., Pan, Z., Zang, L., Zhu, Y., Yin, J., and Gong, W.: Opposing
795 comparable large effects of fine aerosols and coarse sea spray on marine warm clouds,
796 Communications Earth & Environment, 3, 232, 10.1038/s43247-022-00562-y, 2022.
797 Lolli, S., Sicard, M., Amato, F., Comeron, A., Gíl-Diaz, C., Landi, T. C., Munoz-Porcar, C., Oliveira,
798 D., Dios Otin, F., Rocadenbosch, F., Rodriguez-Gomez, A., Alastuey, A., Querol, X., and Reche, C.:
799 Climatological assessment of the vertically resolved optical and microphysical aerosol properties
800 by lidar measurements, sunphotometer, and in-situ observations over 17 years at UPC
801 Barcelona, EGUsphere, 2023, 1-29, 10.5194/egusphere-2023-893, 2023.
802 Miltenberger, A. K., Field, P. R., Hill, A. A., Rosenberg, P., Shipway, B. J., Wilkinson, J. M., Scovell,
803 R., and Blyth, A. M.: Aerosol–cloud interactions in mixed-phase convective clouds – Part 1:
804 Aerosol perturbations, Atmos. Chem. Phys., 18, 3119-3145, 10.5194/acp-18-3119-2018, 2018.
805 Molod, A., Takacs, L., Suarez, M., and Bacmeister, J.: Development of the GEOS-5 atmospheric
806 general circulation model: evolution from MERRA to MERRA2, Geosci. Model Dev., 8, 1339-1356,
807 10.5194/gmd-8-1339-2015, 2015.
808 Ou, Y., Li, Z., Chen, C., Zhang, Y., Li, K., Shi, Z., Dong, J., Xu, H., Peng, Z., Xie, Y., and Luo, J.:

Evaluation of MERRA-2 Aerosol Optical and Component Properties over China Using SONET and PARASOL/GRASP Data, Remote Sensing, 14, 821, 2022.

Pan, Z., Mao, F., Rosenfeld, D., Zhu, Y., Zang, L., Lu, X., Thornton, J. A., Holzworth, R. H., Yin, J., Efraim, A., and Gong, W.: Coarse sea spray inhibits lightning, Nat Commun, 13, 4289, 10.1038/s41467-022-31714-5, 2022.

Radhakrishna, B., Satheesh, S., Narayana Rao, T., Saikranthi, K., and Sunilkumar, K.: Assessment of DSDs of GPM-DPR with ground-based disdrometer at seasonal scale over Gadanki, India, Journal of Geophysical Research: Atmospheres, 121, 2016.

Randles, C. A., Da Silva, A. M., Buchard, V., Colarco, P. R., Darmenov, A., Govindaraju, R., Smirnov, A., Holben, B., Ferrare, R., Hair, J., Shinozuka, Y., and Flynn, C. J.: The MERRA-2 Aerosol Reanalysis, 1980 - onward, Part I: System Description and Data Assimilation Evaluation, J Clim, 30, 6823-6850, 10.1175/jcli-d-16-0609.1, 2017.

Rosenfeld, D., Lohmann, U., Raga, G. B., O'Dowd, C. D., Kulmala, M., Fuzzi, S., Reissell, A., and Andreae, M. O.: Flood or Drought: How Do Aerosols Affect Precipitation?, Science, 321, 1309-1313, 10.1126/science.1160606, 2008.

Smalley, K. M. and Rapp, A. D.: The Role of Cloud Size and Environmental Moisture in Shallow Cumulus Precipitation, Journal of Applied Meteorology and Climatology, 59, 535-550, https://doi.org/10.1175/JAMC-D-19-0145.1, 2020.

Sun, E., Xu, X., Che, H., Tang, Z., Gui, K., An, L., Lu, C., and Shi, G.: Variation in MERRA-2 aerosol optical depth and absorption aerosol optical depth over China from 1980 to 2017, Journal of Atmospheric and Solar-Terrestrial Physics, 186, 8-19, https://doi.org/10.1016/j.jastp.2019.01.019, 2019a.

Sun, E., Che, H., Xu, X., Wang, Z., Lu, C., Gui, K., Zhao, H., Zheng, Y., Wang, Y., Wang, H., Sun, T., Liang, Y., Li, X., Sheng, Z., An, L., Zhang, X., and Shi, G.: Variation in MERRA-2 aerosol optical depth over the Yangtze River Delta from 1980 to 2016, Theoretical and Applied Climatology, 136, 363-375, 2019b.

Sun, N., Fu, Y., Zhong, L., and Li, R.: Aerosol effects on the vertical structure of precipitation in East China, npj Climate and Atmospheric Science, 5, 60, 10.1038/s41612-022-00284-0, 2022.

Sun, Y. and Zhao, C.: Distinct impacts on precipitation by aerosol radiative effect over three different megacity regions of eastern China, Atmos. Chem. Phys., 21, 16555-16574, 10.5194/acp-21-16555-2021, 2021.

Wang, M., Zhao, K., Xue, M., Zhang, G., Liu, S., Wen, L., and Chen, G.: Precipitation microphysics characteristics of a Typhoon Matmo (2014) rainband after landfall over eastern China based on polarimetric radar observations, Journal of Geophysical Research: Atmospheres, 121, 2016.

Xiao, Z., Zhu, S., Miao, Y., Yu, Y., and Che, H.: On the relationship between convective precipitation and aerosol pollution in North China Plain during autumn and winter, Atmospheric Research, 271, 106120, https://doi.org/10.1016/j.atmosres.2022.106120, 2022.

Yang, Y., Wang, R., Chen, F., Liu, C., Bi, X., and Huang, M.: Synoptic weather patterns modulate the frequency, type and vertical structure of summer precipitation over Eastern China: A perspective from GPM observations, Atmospheric Research, 249, 105342, https://doi.org/10.1016/j.atmosres.2020.105342, 2021.

Yuan, T., Remer, L. A., Pickering, K. E., and Yu, H.: Observational evidence of aerosol enhancement of lightning activity and convective invigoration, Geophysical Research Letters, 38, https://doi.org/10.1029/2010GL046052, 2011.

Zhang, A., Chen, Y., Zhang, X., Zhang, Q., and Fu, Y.: Structure of Cyclonic Precipitation in the Northern Pacific Storm Track Measured by GPM DPR, Journal of Hydrometeorology, 21, 227-240, https://doi.org/10.1175/JHM-D-19-0161.1, 2020a.

Zhang, Y., Yu, F., Luo, G., Chen, J.-P., and Chou, C. C. K.: Impact of Mineral Dust on Summertime Precipitation Over the Taiwan Region, Journal of Geophysical Research: Atmospheres, 125, e2020JD033120, https://doi.org/10.1029/2020JD033120, 2020b.